THE UNIVERSITY OF MICHIGAN

College of Engineering

Department of Mechanical Engineering

Cavitation and Multiphase Flow Laboratory

Report No. 01357-16-T

SOME EFFECTS OF APPLIED STRESS ON EARLY STAGES OF CAVITATION DAMAGE

(1970 Symposium on Fluid Mechanics and Design of Turbomachinery, August 31, September 1-3, 1970, Pennsylvania State University)

by

Dale J. Kemppainen*

Frederick G. Hammitt**

Financial Support Provided by:

National Science Foundation
Grant No. GK-1889

*Formerly Graduate Student, Nuclear Engineering Department, University of Michigan, Ann Arbor, Michigan; present address: Knolls Atomic Power Laboratory, General Electric Company, Schenectady, New York

**Professor-in-Charge, Cavitation and Multiphase Flow Laboratory, Mechanical Engineering Department, University of Michigan

April 1970

I. INTRODUCTION

The problem of material attrition due to the phenomenon of cavitation has become increasingly more important in recent years. Methods of alleviating cavitation damage have been suggested, including the use of externally applied stresses. The possible presence of inherent tensile or compressive stresses in fluid system components causes concern regarding their effect on the longevity of the components of the system as a whole when exposed to cavitation. Previous work from this laboratory[1] indicated that the effect of stress upon cavitation damage rates depended strongly upon the material. In general, compression, if applied parallel to the surface, tended to reduce the damage, and tension to increase it. The present paper considers particularly the initial phases of damage and what effect these external stresses have on the extent to which damage is incurred.

II. EXPERIMENTAL FACILITIES

A. General

Three experimental facilities were used to procure the data required for this study. These were: 1) water loop with venturi, 2) mercury loop with venturi, and 3) vibratory facility (stationary specimen, nonflow system). Each of these facilities has been extensively discussed elsewhere.[2, 3, 4, 5] A short description of each system is given here only for clarification of test conditions. Reference 2 presents full details.

1. Water loop - the water loop, a multiple, closed-loop system, is shown in Fig. 1. One of the available loops was operated at a venturi throat velocity of 50 f/s at 75°F in the 1/2 in. dia. throat. (1)

2. Mercury loop - the mercury loop (Fig. 2) is a single loop venturi system. A throat velocity of 30 f/s at 75°F in the 1/2 in. dia. throat was used. (2)

3. Vibratory facility - a standard exponential horn (20 kHz, 2 mil) was used. The test specimens were held stationary in the cavitation field about 18 mils from the oscillating horn tip. Fig. 3 is a schematic diagram of one of the (3)
arrangements used, and Fig. 4 of the other. (4)

B. Specimen Placement

In both flowing systems a cylindrical specimen (Fig. 5) was (5)
used. The specimen was placed across the fluid stream in the venturi diffuser, (Fig. 6), slightly downstream from the venturi throat (6)
exit.

Two types of specimens were used in the vibratory facility depending upon the method used to provide the applied stress: a) 1.25 in. dia. slugs placed parallel to the face of the vibratory horn, or b) a specimen of dumb-bell shape, closely resembling a tensile test specimen (Fig. 7). Fig. 4 shows the specimen arrangement. (7)
These tests were run in distilled water at 73°F.

C. Effect of Radially-Symmetric Compressive Stress (Arrangement No. 1)

The first arrangement provides a radially-symmetric compressive surface stress which corresponds to the radially-symmetric flow of the fluid imposed by the oscillating horn tip.[2] This stress field was provided by shrink-fitting an outer ring around the metal center (Fig. 8). The test specimen consisted of a solid cylindrical (8)
center section nominally 0.25 in. thick and 0.7500 $\pm$ 0.0005 in. in dia. of the material to be tested. The outer ring was of 304 stainless steel. By adjusting the radial interference, δ, the calculated specimen stress is varied according to the relationship:

$$P_{sf} = \frac{\delta/b}{\frac{1}{E_o}\left[\frac{1+(b/c)^z}{1-(b/c)^z} + \nu_o\right] + \left[\frac{1-\nu_I}{E_I}\right]}$$

where P_{sf} = compressive stress on the specimen material

E_o = elastic modulus of the ring material

E_I = elastic modulus of the test material

ν_o = Poisson's ratio for the outer material

ν_I = Poisson's ratio for the test material

$b + \delta$ = test specimen radius

δ = radial interference

c = outside radius of the outer ring

b = inside radius of the ring

The specimen and ring combinations were selectively paired according to the difference of fit, δ, after accurate measurement of the diameters, thus providing the desired surface compressive stress to the inner slugs.

D. Materials

Test materials were chosen which exhibited good reproducibility and availability, ease of fabrication, and relatively low damage resistance. Two materials, chosen to obtain rapid damage to investigate the feasibility of the test, were: -- O. F. H. C. (oxygen free high conductivity copper) and 2024 aluminum. Control specimens of these materials were also made to the same diameter as the total test-slug-ring combination. Thus the same flow conditions were maintained for both the controls and compressively-loaded specimens.

III. TEST RESULTS

A. Damage Rates

Fig. 9 (test data obtained for the shrink-fit specimens) indicates that the cavitation damage resistance of both the O. F. H. C. copper and the 2024 aluminum (comparing maximum volumetric loss (9)

rates) is decreased by the impressed radially-symmetric compressive stress (19.3% increase in damage over the non-stressed control for the copper and 7.1% for the aluminum). However, the initial damage rate (i.e., that between time zero and 15 minutes) for the aluminum of the compressed specimen was less than that for the non-stressed specimen. This same effect was reported earlier[1, 2] for a number of other materials stressed only in the axial direction. For this particular material, in this test, for mean depth of penetration, MDP* $<$ 0.1 mils, the effect of the radially-symmetric compressive stress was thus to inhibit the amount of cavitation damage. For greater MDP the damage rate increases, indicating that after the initial damage period the inhibiting effect of the compressive stress decreases and then becomes negative. Thus the compressive stress appears to be detrimental once the surface of the material has been broken.

These same trends were not seen in the copper. However, no measurements for $<$0.1 mil MDP were made.

B. Photographic Investigation of Short Duration Damage Tests

The results of a photographic investigation of specimens under three load conditions, (i.e., tension, compression and zero applied load) are shown in Fig. 10-a, b, c. These photographs are each a composite of 10-deg. segments of a cylindrical specimen (Fig. 5) run in the mercury loop (Fig. 2). The test duration was 1.5 min. with a throat velocity of 30 f/s and a pressure drop across the venturi of 71 psi. The pitting density changes which are evident from sector to sector are due to the distribution of the cavitation field which (10)

*MDP = Mean Depth of Penetration, i.e., the volume loss/unit area, or an equivalent damage depth if volume loss were uniform across the entire area.

$$MDP = \frac{W}{\rho A}$$

where: W = weight loss
ρ = density
A = damage area over which weight loss occurs

surrounds the specimen in this configuration.[6] Fig. 10-a shows a polished 304 stainless steel specimen tested with zero applied stress. Fig. 10-b shows the same material tested under a compressive load parallel to its axis of 88% of its yield strength, while Fig. 10-c is for an impressed tensile load of 88% of the yield strength.

Comparing the photo for the imposed compressive force (Fig. 10-b) with that for zero force (Fig. 10-a) shows a very significant reduction in the number of smaller size pits, and some reduction for all pits for compressive load. There are, however, still some very large pits visible in the compressive specimen. The tensile specimen (Fig. 10-c) and the zero force specimen (Fig. 10-a) appear to be quite similar in pit number densities of all sizes.

Three highly-polished brass (65/35) specimens were run in the vibratory rig under conditions of tensile, compressive, and zero external applied load. The test duration in each stress mode was 10 sec. The results are shown in Fig. 11-a, b, c. As in Fig. 10, (11)
there is markedly less pitting for compressive applied load than for other conditions. Under microscopic examination, all specimens showed approximately uniform damage distribution over the damaged area. For comparison, Fig. 12 shows a heavily damaged specimen. (12)
Proficorder traces across its damaged area indicate that damage depth is again approximately uniform.[2]

Comparing the short duration specimens in detail, the pit number density is greatest for the tension specimen (Fig. 11-a). There are a greater number of small pits than of large as is typical in cavitation tests. The specimen with zero applied load (Fig. 11-b) has a somewhat larger number of small pits than the tension specimen, but the number and size of large pits is about the same. The compressive specimen (Fig. 11-c), however, shows a definite decrease

in the number of both small and large pits.

Comparing the results from the vibratory facility with those from the mercury loop, the effect of externally applied stress are about the same, even though specimen shape, material and fluid properties, and cavitation field differed drastically. In both tests the effect of the compression upon damage in the early stages is to strongly decrease the number of small pits, with less effect upon larger pits. Even in the early stages, however, the compressive force does not totally alleviate the damage. Rather it appears to increase the threshold bubble energy required for creating a pit, thereby decreasing most strongly the number of small pits. The material is still vulnerable to higher energy bubble collapses, which cause the larger pits. It thus appears that the "incubation period" is increased by a compressive pre-load.

Additional examples of early damage on metallic specimens were obtained using a plated specimen of 304 stainless steel. This experiment was suggested by the previous work of Noell[7] and Wood[8] who used a lacquer film coating to indicate quickly areas of maximum vulnerability to cavitation damage. Our water loop and associated test venturi were used in this investigation. Venturi throat velocity was 50 f/s with the cylindrical specimen (Fig. 5) placed across the venturi. Several lacquer coatings were investigated. However, since these did not provide adequate bonding to the 304 stainless steel specimen, electroplated cadmium films of various thicknesses were tried. These plated specimens were exposed to the cavitation field of the venturi for a 15 min. duration, and then examined microscopically. As in the previously described mercury tests, the damage appeared on the side and downstream portion of the cylinders. Pressure profiles and flow regime photographs which enabled prediction of these damage areas were reported previously.[2,6] Unlike the specimen from the mercury loop, only a

small number of distinct circular holes or pits were found. Fig. 13 shows the effect of varying thickness of the cadmium plate. A (13)
complete removal of cadmium at the pit center occurred for the thinner platings (Fig. 13-a, b). For thicker plating (Fig. 13-c), the damage does not extend completely through the plating.

In Fig. 13-b a raised rim around the circular damaged area appears. Fig. 13-c shows areas where the cadmium has been partially disloged. Close examination of these pits (Fig. 13-c) shows small circular areas (indicated by arrows and outlined in black ink for easier visualization) near the center of the damaged areas suggesting a very local circular area of most intense attack, as if the surface had been impacted by a microjet of liquid.

Fig. 14 shows more detail of the pits in the thinner platings. (14)
The central area of each pit, void of all plating material, is surrounded by an outer area from which only a minor portion of the plating has been removed. Fig. 14-a is an enlarged photo of the most central pit in Fig. 13-a. Its diameter is 0.6 μm. The complete symmetry of this central region from which the cadmium has been removed is shown. Such excellent symmetry strongly indicates that the material removal has been accomplished by a single (rather than multiple) impact.

These pictures strongly substantiate the theory that cavitation damage even in a flowing system may be created by liquid microjets generated during bubble collapse, rather than by spherical shock waves radiating from the bubble collapse center. The type of damage shown cannot easily be attributed to such shock waves which would merely press the cadmium plate into the surface, (as was demonstrated by impacting steel shot against a similar surface), rather than "washing it off". This damage is much more easily understood as the result of the radial velocity from a high velocity impacting

liquid jet. Selected pictures of this type have been published previously from this laboratory[9] in support of this theory.

C. Metallurgical Examination of Damage Pits

A metallurgical examination of the region of the damaged surfaced area of the tension and compression specimens was made. SAE 660, a cast bearing bronze, and O. F. H. C. copper were tested for this purpose in the vibratory rig. Test duration was sufficient to provide relatively large MDP. Fig. 15 illustrates the method of (15) sectioning. The specimens were polished, etched, and then photographed at 400 diameters.

Fig. 16 is four photomicrographs of a damaged SAE 660 (16) specimen, showing both transverse and longitudinal sections. The interior "holes" are porosity in the cast material. This specimen had been tested under zero applied load. In the section in the transverse direction (Fig. 16-a and b) only a few cracks are visible. Slip lines, however, can be seen in photograph A at the base of the pit on the top right. Slip lines are also visible in photographs B, C, and D, indicating that the material adjacent to the pits has experienced considerable cold work. In photographs A and B the slip lines appear almost perpendicular to the pit apex.

The longitudinal photographs (Fig. 16-c and d) show some evidence of microcracks at the base of the pits. In the center of photograph D a large pit has at its apex a number of microcracks emanating in different directions. There are also slip lines on either side of the pitted region, and particularly to the right of the apex, indicating that considerable cold work was done in this region. Fig. 17 shows photomicrographs of an SAE 660 specimen tested under com- (17) pressive load, while C and D are for a tensile specimen. In both stress modes the longitudinal pictures show the microcracks from the area of the pit apex running vertically to the surface, and the transverse

pictures show the microcracks angled off from the pitted surface, None of these photos show slip lines, and there is no apparent difference between specimens tested under compressive or tensile load.

Fig. 18, photos A and B, show a copper specimen damaged with zero applied force, and C and D a copper specimen damaged under tunsile load. In A and B there appears to be no difference between the transverse direction (A) and the longitudinal direction (B). There are, however, a few small microcracks at or near the apex of the damage pits. There are no discernable slip lines in these photographs, perhaps indicating little or no work hardening of the damaged surface. (18)

Photos C and D also show no slip lines. However, both the transverse (C) and the longitudinal (D) direction show larger more prominent microcracks emanating from the base of the damage pits. As for the SAE 660, the cracks in the longitudinal direction appear to come away from the pits at an angle almost perpendicular to the centerline of the pit.

Fig. 19 shows both the transverse (A) and the longitudinal (B) directions of a copper specimen cavitated in compression. Close examination of the photographs shows a number of microcracks at the base of the damage pits. These seem to start at the apex of the pit and continue until they intersect a grain boundary, at which point they terminate. The longitudinal picture again shows the direction of the cracks to be perpendicular to the surface. (19)

Photomicrographs (not shown) for brass specimens give results typical of those for copper. There were, in all cases, microcracks in the region of the damage pits, but no slip lines. The damage is thus accompanied by two possible effects: 1) microcracks emanating from the base of the damage pits and 2) cold work or

strain-hardening depending upon the material just below the damage surface. There appears to be no difference in the number of microcracks or their appearance in specimens tested under compression, tension or zero load for these relatively heavily damaged specimens. This is consistent with the previously stated finding that after the surface has been broken the effect of the externally applied compressive stress is diminished.

IV. CONCLUSIONS

A substantial decrease in the number density of small pits, in the early portion of a test when the materials were subjected to an external compressive stress has been found. There was little difference between tests run under compression between the mercury facility and the vibratory facility. The application of a tensile load in both the mercury facility and the vibratory facility caused very little or no difference in the amount of damage compared to that while under zero load.

Photographic investigation of individual pits shows that they are approximately circular. These photographs strengthen the hypothesis that these pits result from the impact of liquid microjets generated during bubble collapse rather than by spherical shock waves radiating from the center of collapse.

Photomicrographs of different materials indicate two manifestations of damage immediately beneath the surface: 1) microcracks emanating from the apex of the pit, and 2) areas of cold work just adjacent to the pit, depending upon the material used.

The effect of an externally applied compressive stress appears to be diminished after the damage has initially disrupted the surface. This is apparent since little or no differences in the microstructure below the pits was seen for the different stress modes after substantial damage was incurred.

REFERENCES

1. Kemppainen, D. J., and Hammitt, F. G., "Effects of External Load on Cavitation Damage", Proc. IAHR Symposium, Kyoto, Japan, Sept., 1969; also available as ORA Tech. Report 01357-5-T, Mechanical Engr. Dept., University of Michigan.

2. Kemppainen, D. J., "Prestress Conditioning and its Effects on Material Attrition in a Cavitating Environment", Professional Engineering Degree Dissertation, Nucl. Engr. Dept., University of Michigan, June, 1969; also available as ORA Report 01357-7-T, University of Michigan.

3. Garcia, R., "Comprehensive Cavitation Damage Data for Water and Various Liquid Metals Including Correlations with Material and Fluid Properties", Ph. D. thesis (also available as ORA Technical Report 05031-6-T), Department of Nuclear Engr., University of Michigan, August, 1966.

4. Robinson, M. J., "On the Detailed Flow Structure and Corresponding Damage to Test Specimens in a Cavitating Venturi", Ph. D. thesis (also available as ORA Technical Report No. 03424-16-T), Department of Nuclear Engr., University of Michigan, August, 1965.

5. Hammitt, F. G., Kemppainen, D. J., "Cavitating Flow Past Transverse Cylinder in Venturi Diffuser with Water and Mercury , Proc. 3rd Conference on Hydraulics and Hydraulic Machinery, Budapest, Hungary, September, 1969, pp. 255-264.

6. Noell, G. L., "Cavitation Sensitive Coating Evaluation", Pratt and Whitney Aircraft-CANAL, Tech. Info. Memo. No. 878, June, 1965.

7. Wood, G. M., Kulp, R. S., and Altieri, J. V., Jr., "Cavitation Damage Investigations in Mixed Flow Liquid Metal Pumps", Pratt and Whitney Aircraft-CANAL, Symposium on Cavitation in Fluid Machinery, Winter Annual Meeting ASME, Chicago, November, 1965.

8. Hammitt, F. G., Lafferty, J. F., Cheesewright, R., Pitek, M. T., Kemppainen, D. J., and Mitchell, T. M., "Laboratory Scale Devices for Rain Erosion Simulation", Proc. 2nd Meersburg Conference on Rain Erosion (also available as ORA Report 08153-3-T, Department of Nuclear Engr., University of Michigan, March, 1967.

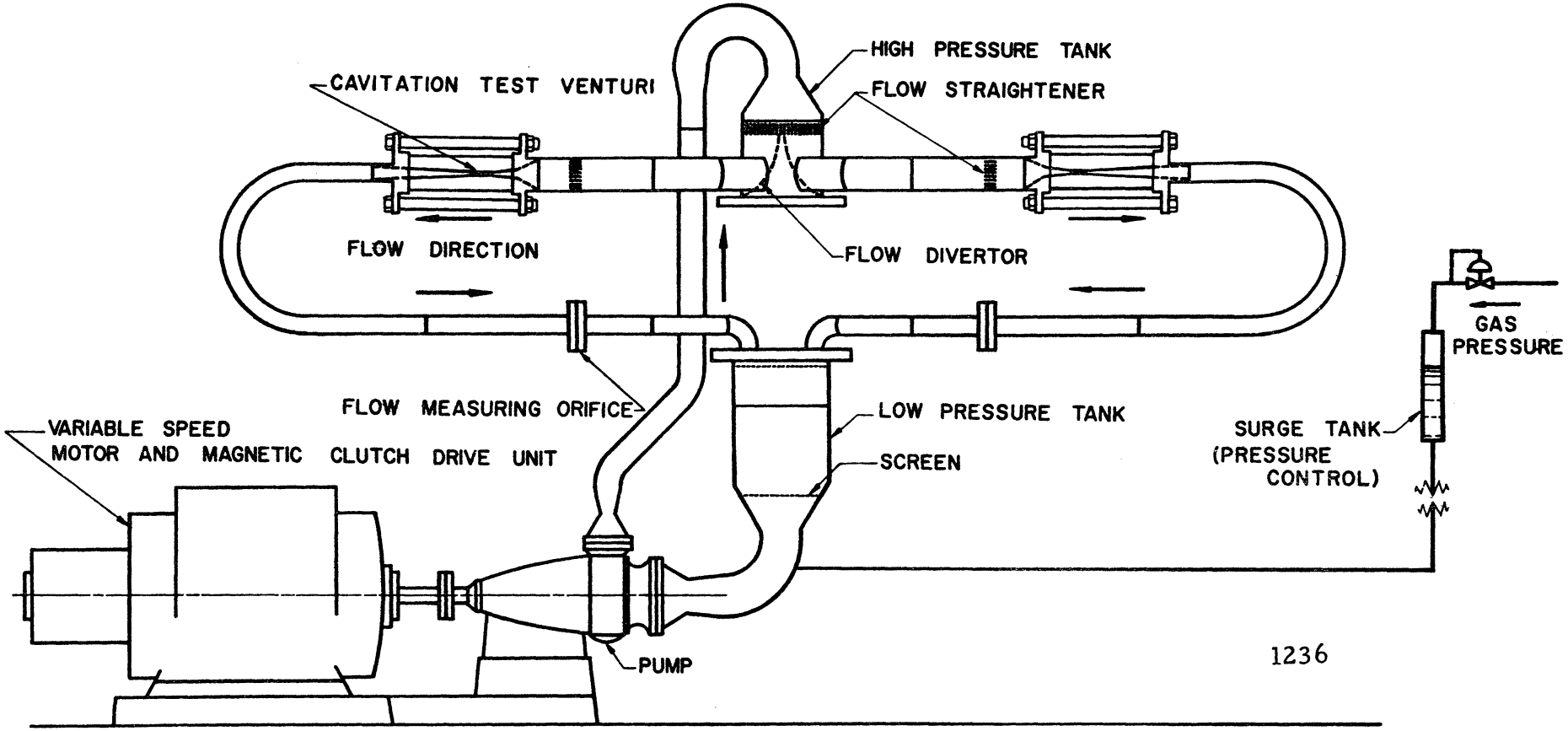

Figure 1. Schematic of Water Cavitation Damage Facility
(only two of the four loops shown)

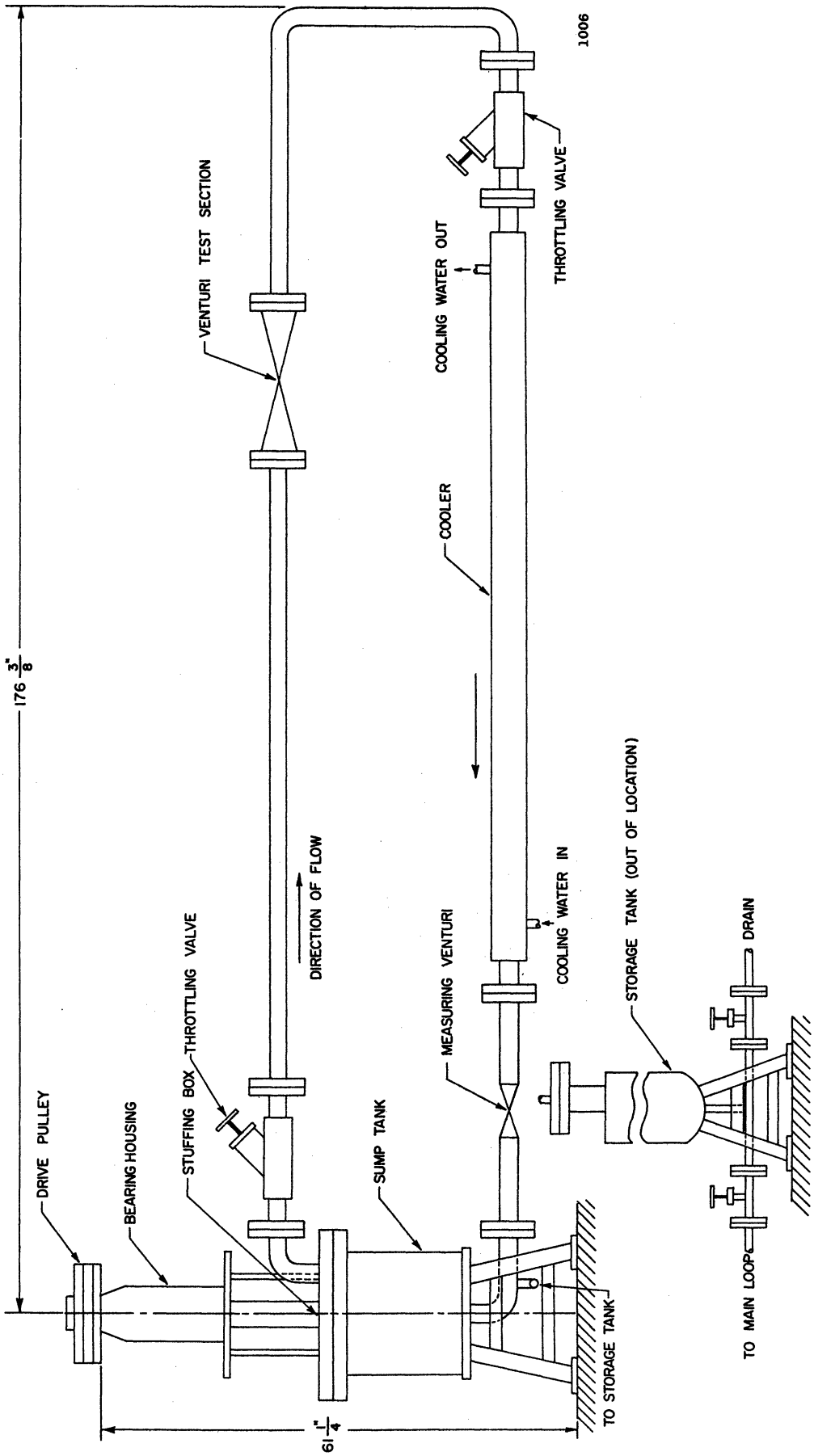

Figure 2. Schematic Drawing of Overall Mercury Facility Layout

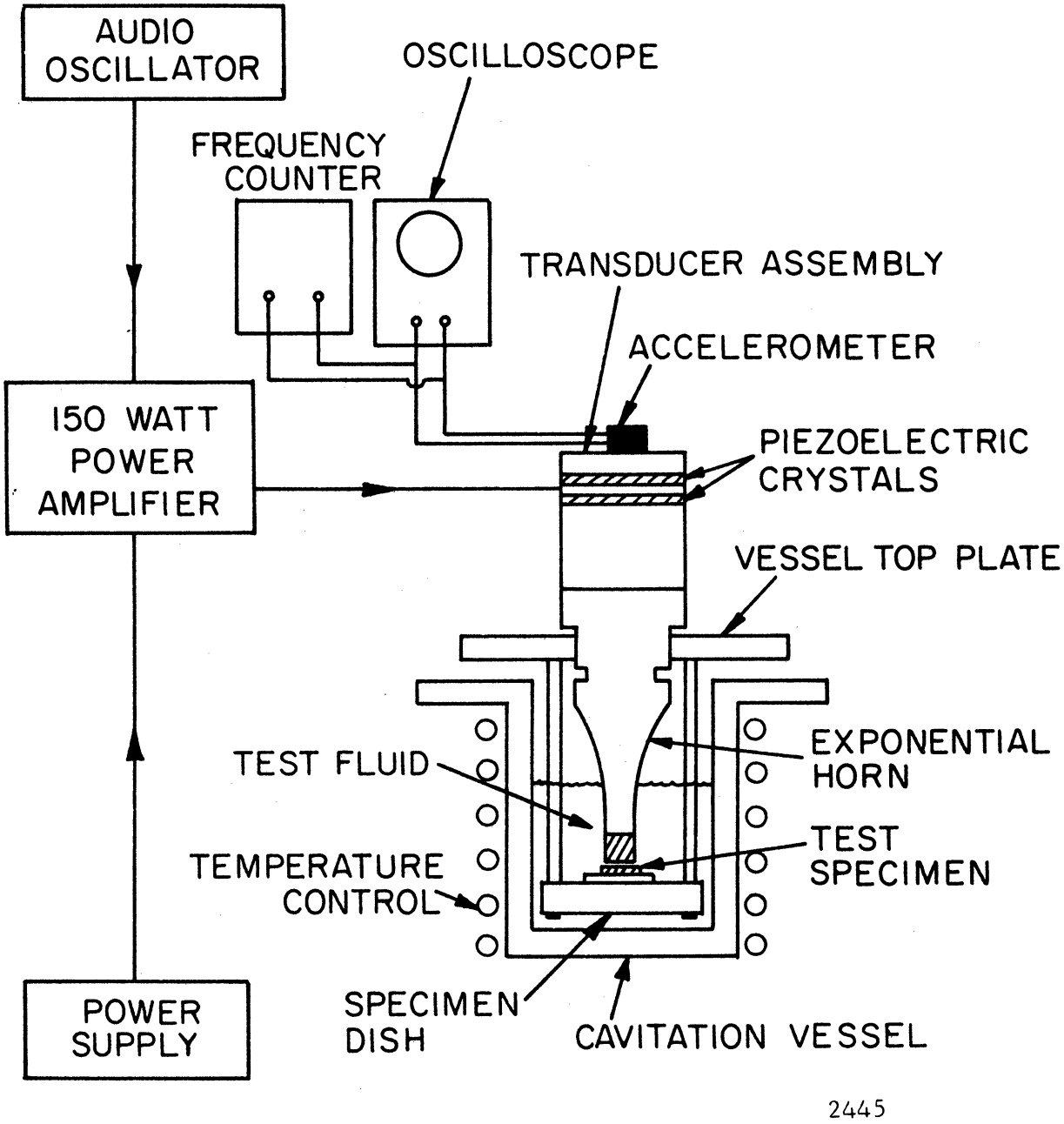

Figure 3. Schematic Representation of the Stationary Specimen Vibratory Cavitation Test Facility

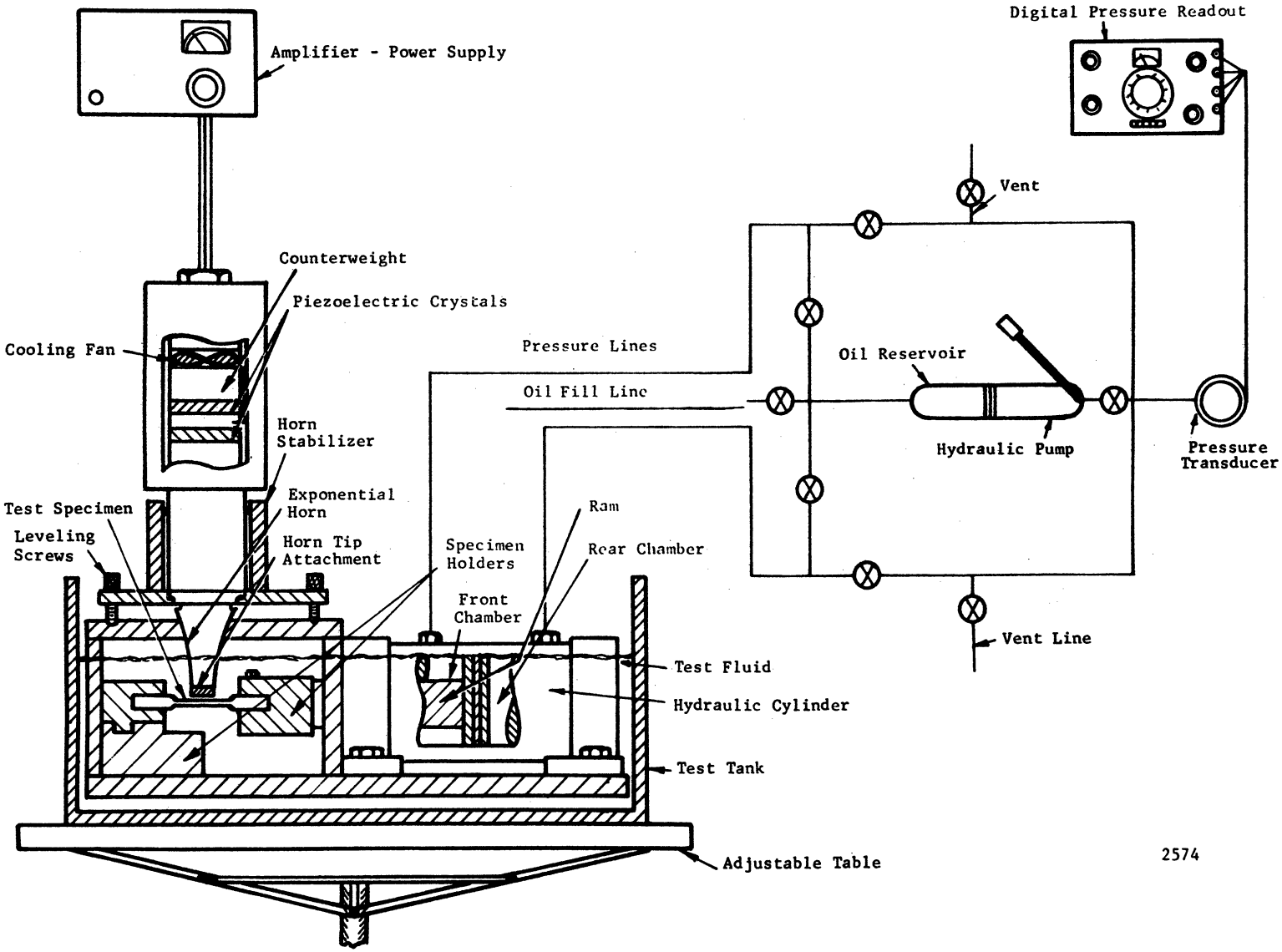

Figure 4. Schematic Diagram of Test Facility

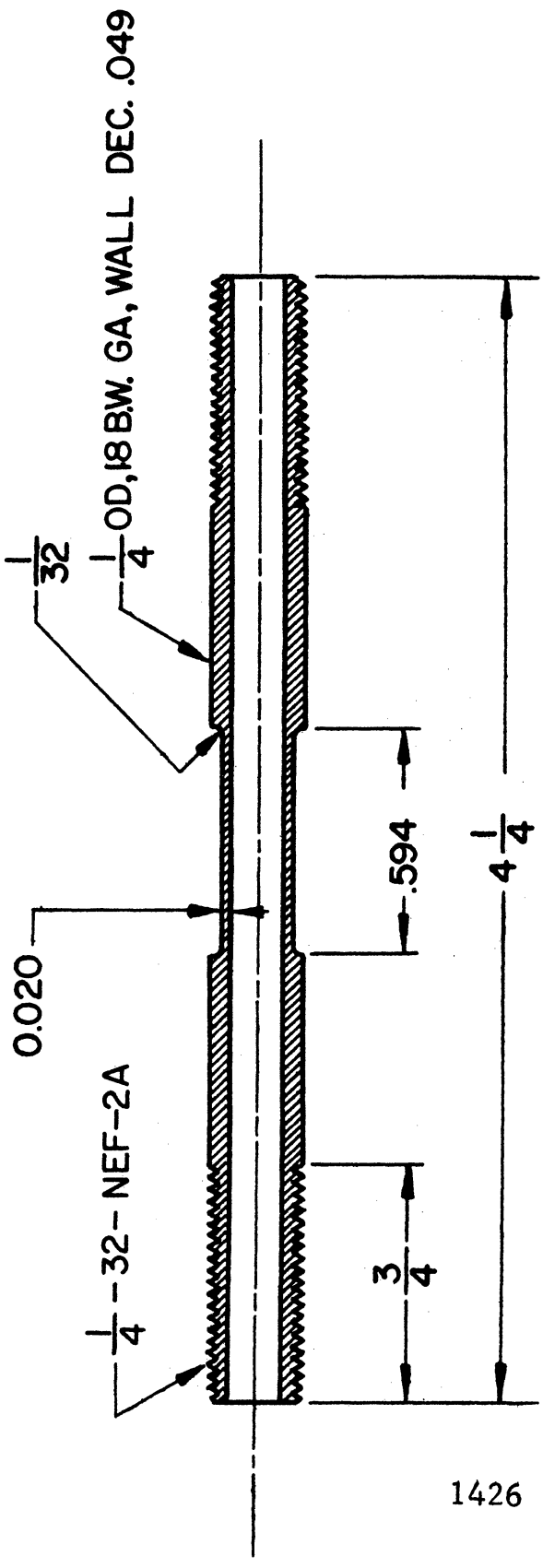

Figure 5. Drawing of Tubular Test Specimen (pin)

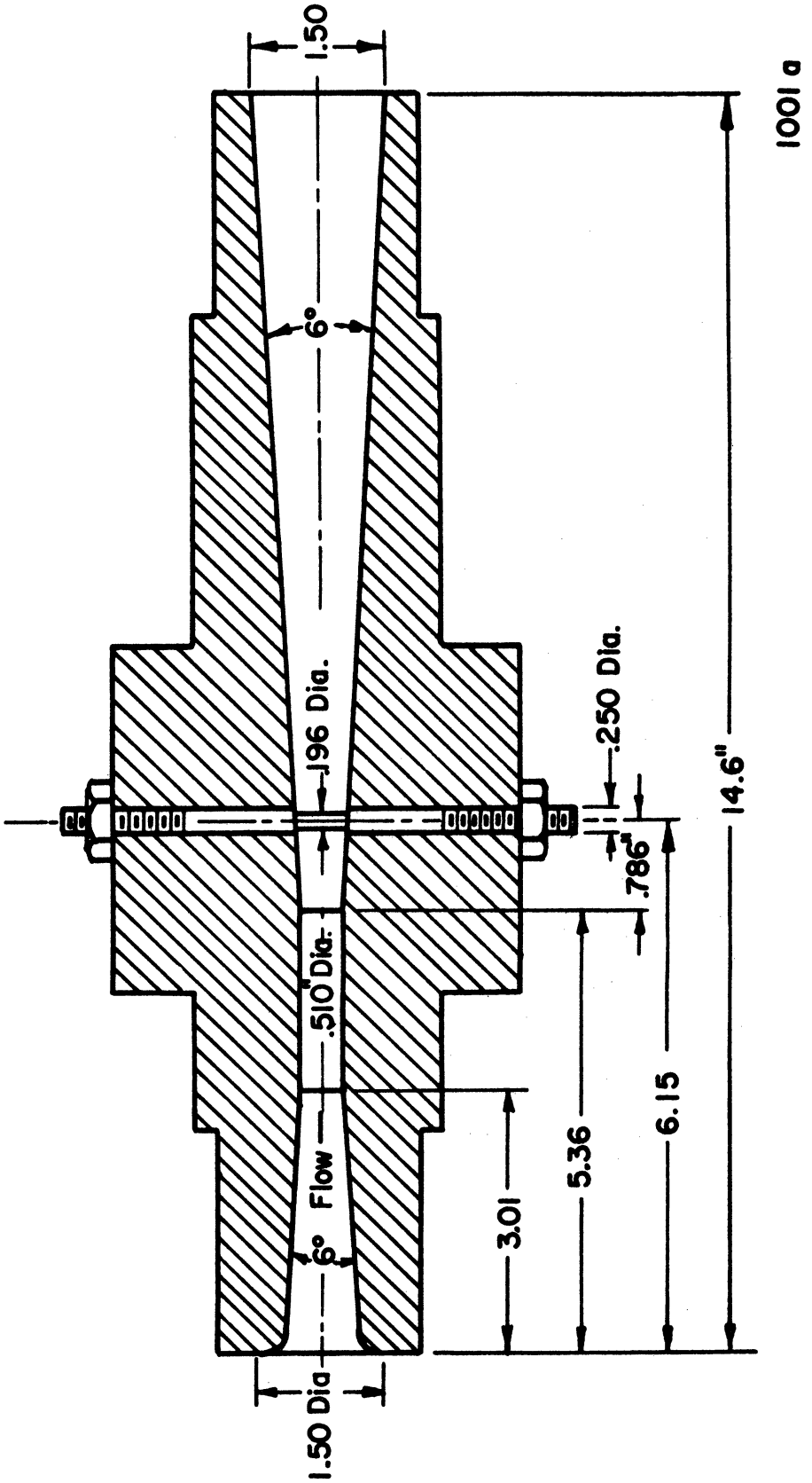

Figure 6. Assembly Drawing of Tension Test Venturi

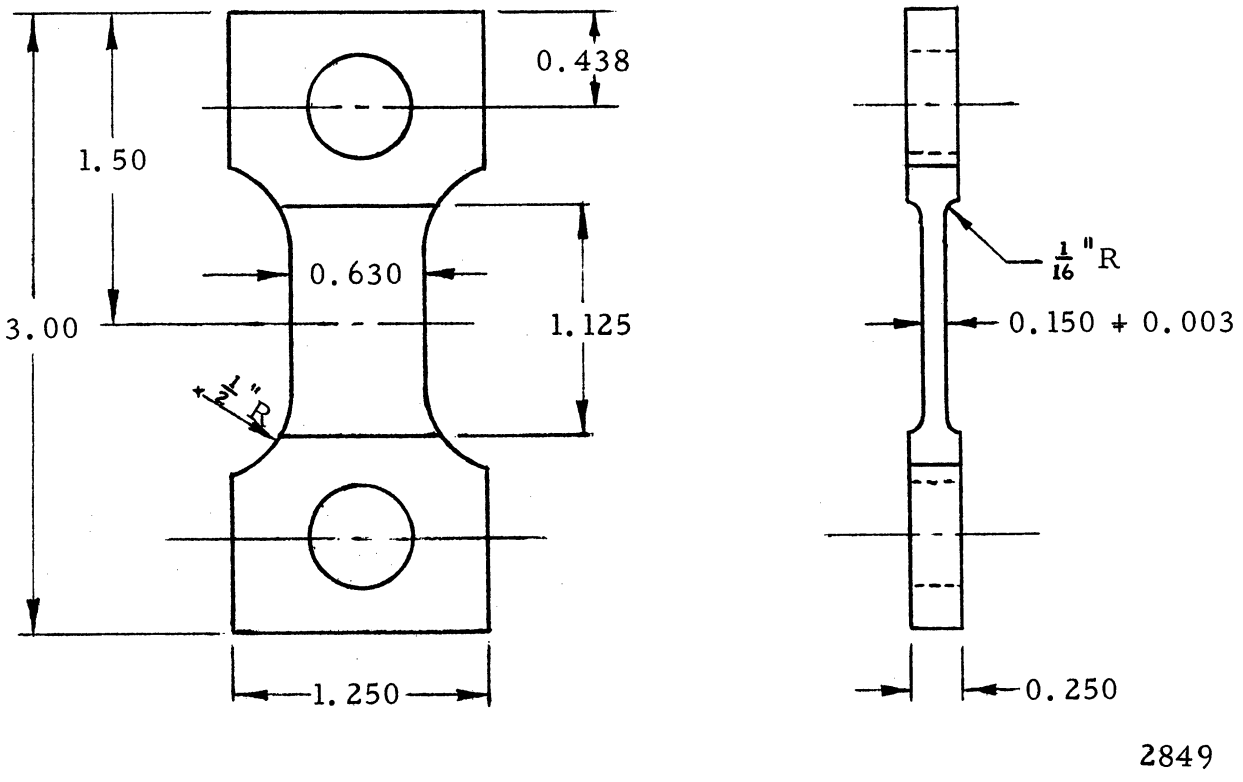

Figure 7. Dimensional Drawing of Tension-Compression Specimen

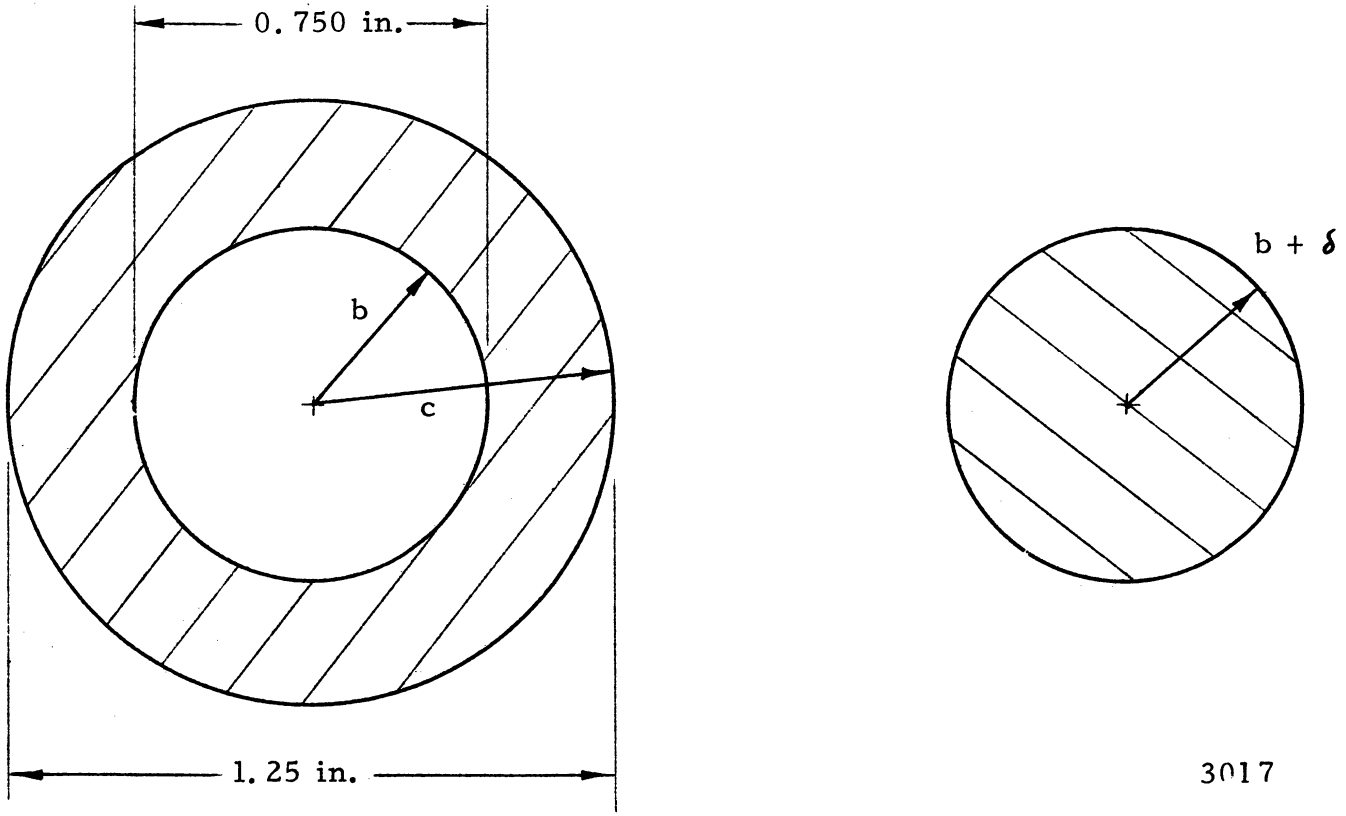

Figure 8. Test Specimen and Ring

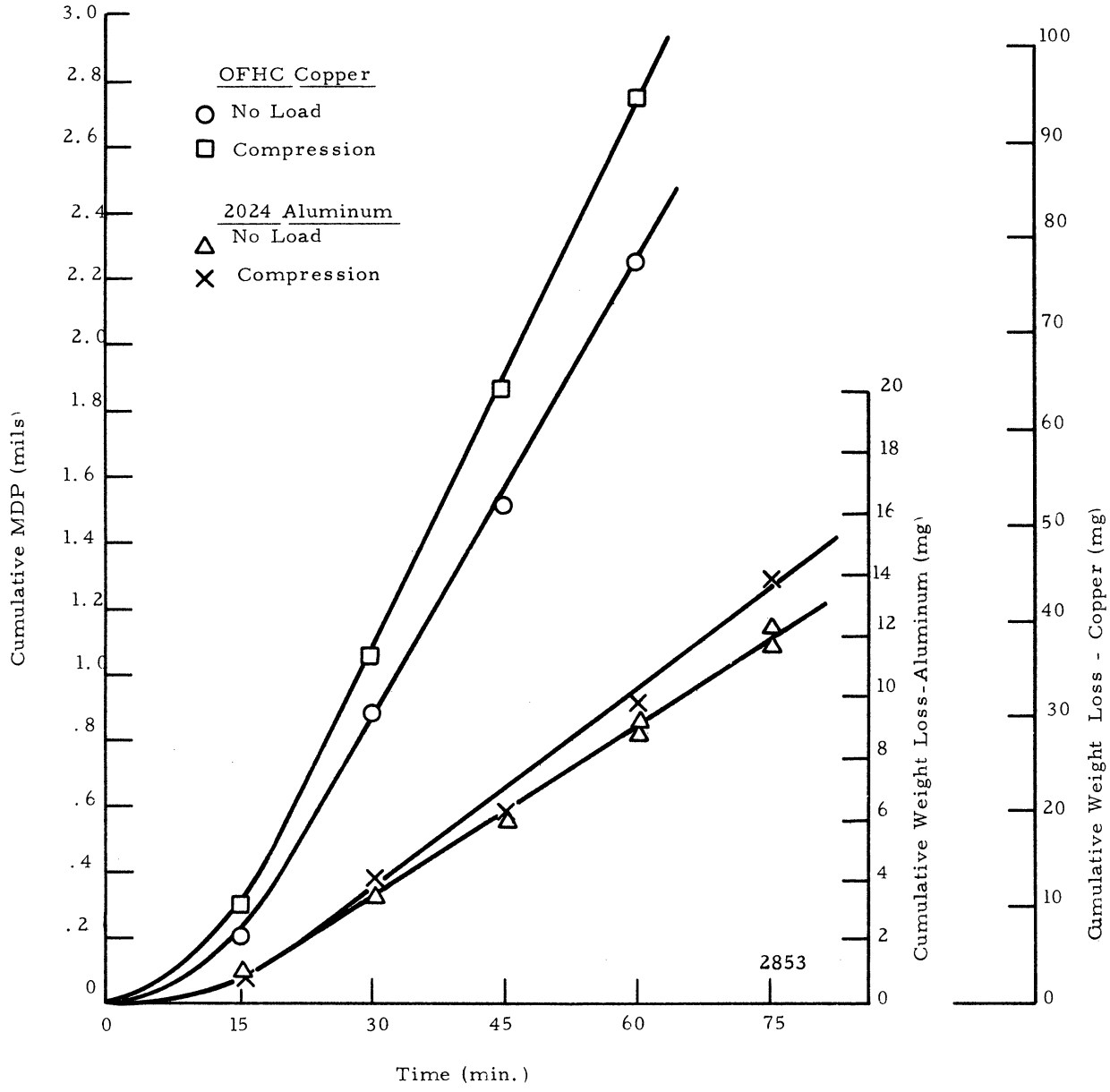

Figure 9. Effect of Compressive Stress on Cumulative Damage of OFHC Copper and 2024 Aluminum Shrink Fit Specimens

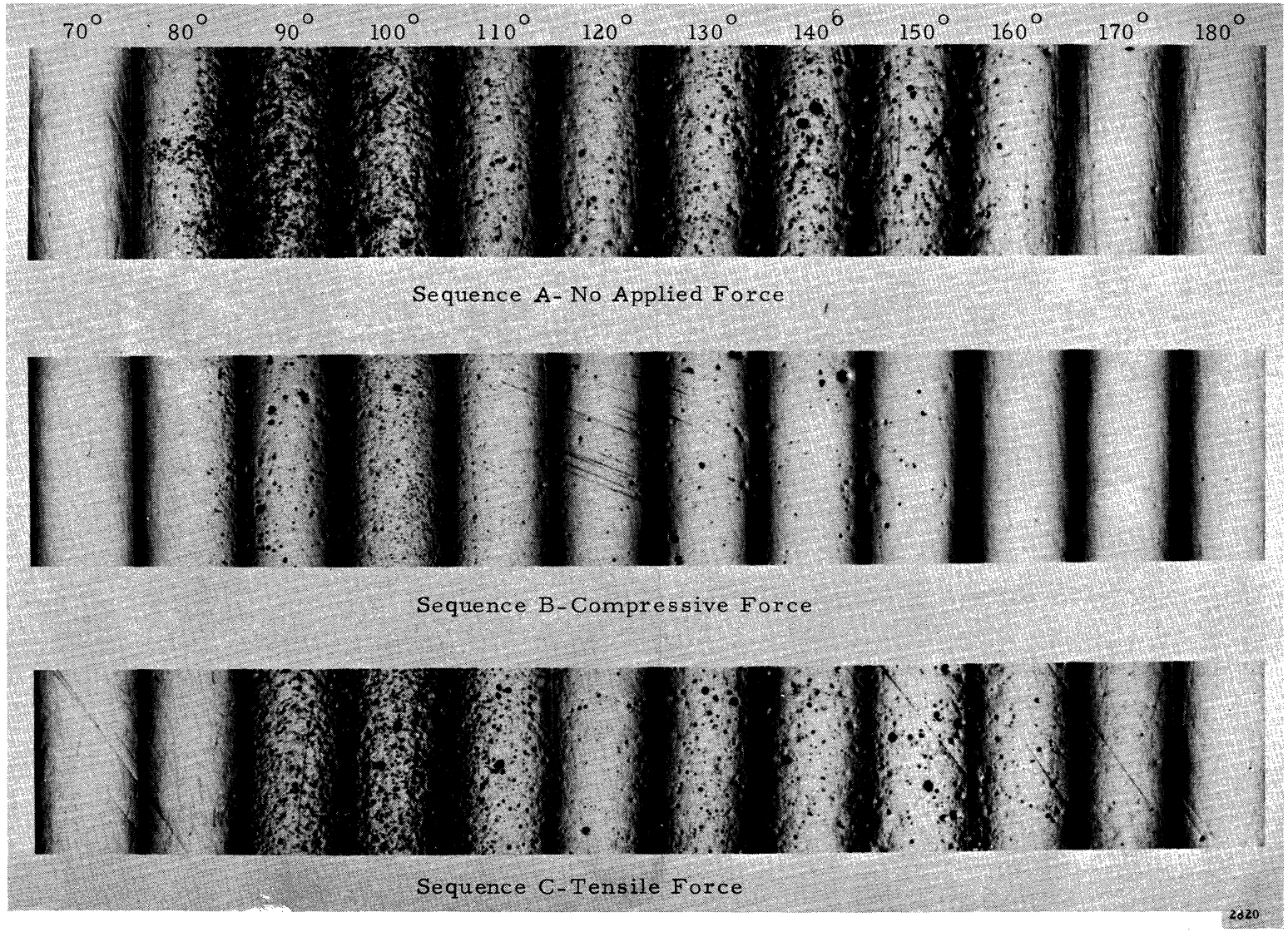

Figure 10. Effect of Surface Stress on Damage for Short Duration Tests

Figure 11a. Cavitation Damage in Tension Brass Vibratory Specimens after 10 sec. Exposure (100x)

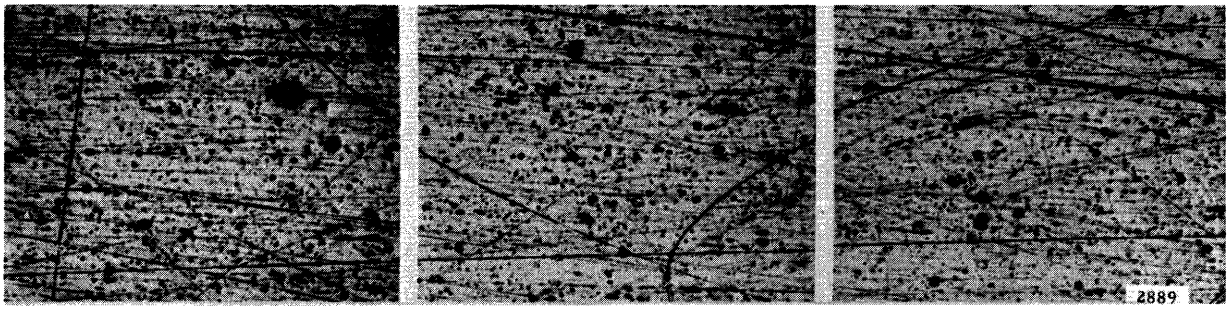

Figure 11b. Cavitation Damage in Zero Load Brass Vibratory Specimens after 10 sec. Exposure (100x)

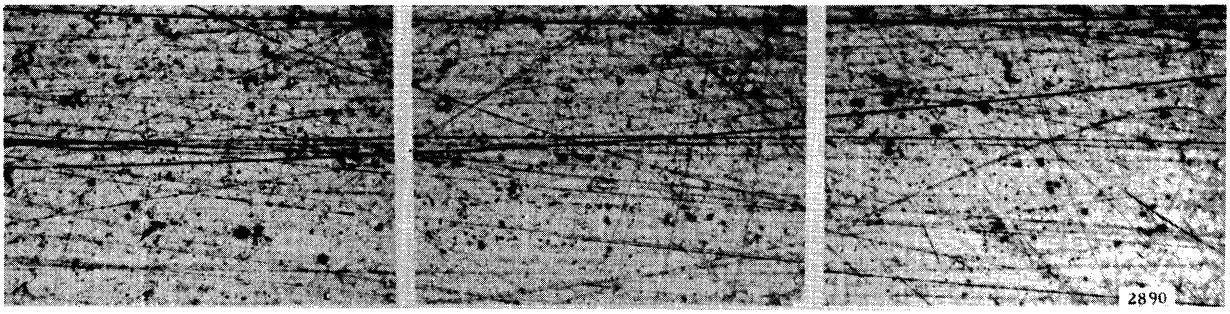

Figure 11c. Cavitation Damage in Compression Brass Vibratory Specimens after 10 sec. Exposure (100x)

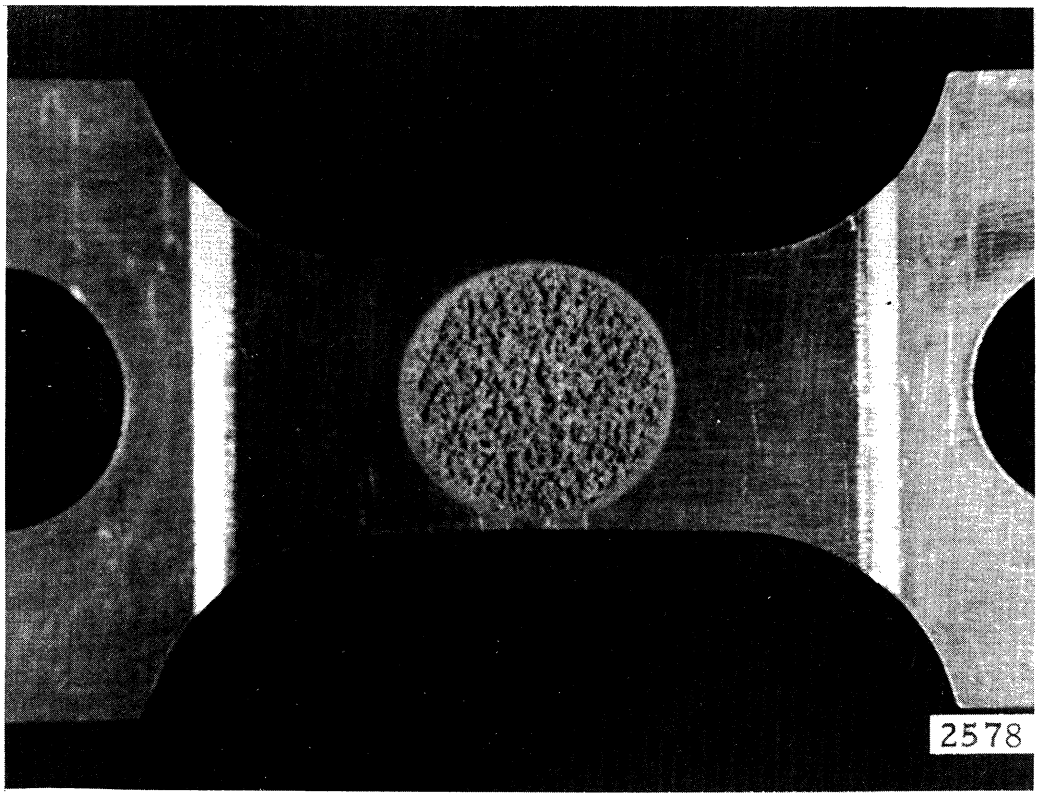

Figure 12. Center Damage Area of a Specimen with a Reduced Cross Section Prior to Tensile Pull

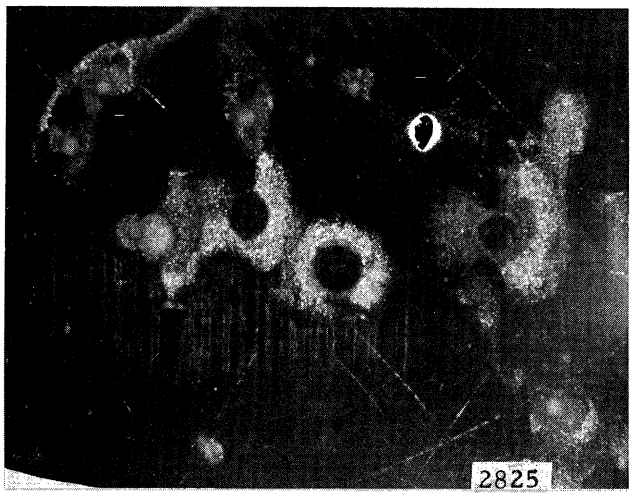

A

Coating Thickness: 2.5×10^{-5} in.

(120x)

B

Coating Thickness: 5×10^{-5} in.

Note raised rim.

(120x)

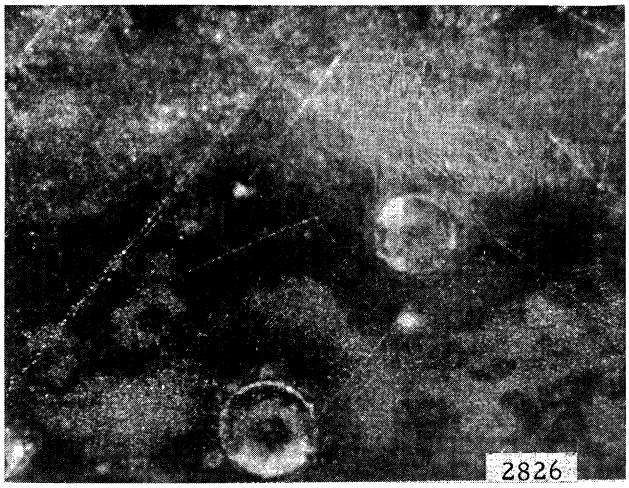

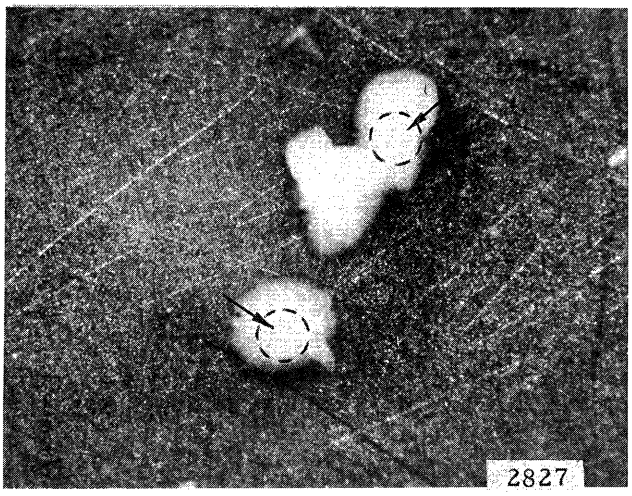

C

Coating Thickness: 5.5×10^{-4} in.

Small circles marked by arrows indicate a point of impact of a central jet.

(120x)

Figure 13. Effect of Increasing Cadmium Coating Thickness of Stainless Steel Tubular Pin Specimens on Water Loop Cavitation Pits

A

Coating Thickness: 2.5×10^{-5} in.

Enlargement of the most central pit in Fig. 26-A.

(500x)

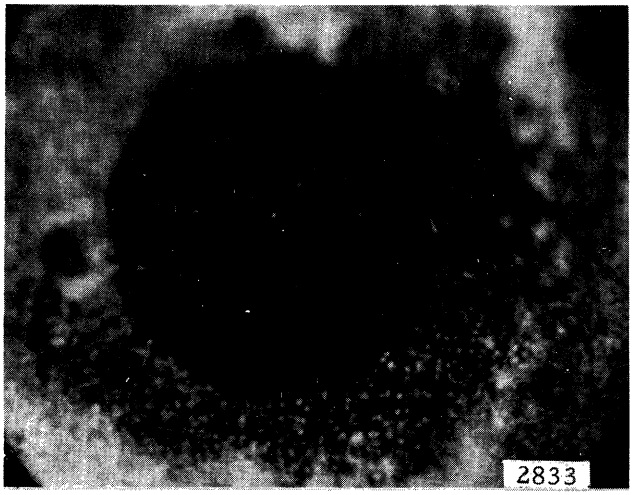

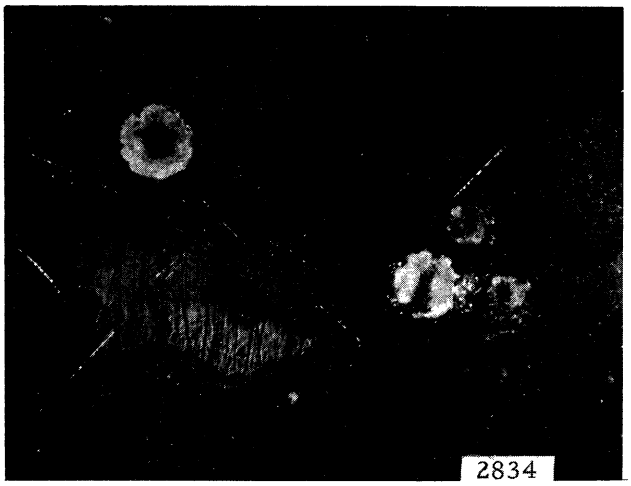

B

Coating Thickness: 5×10^{-5} in.

(120x)

C

Coating Thickness: 5×10^{-5} in.

Note difference in area around pits.

(120x)

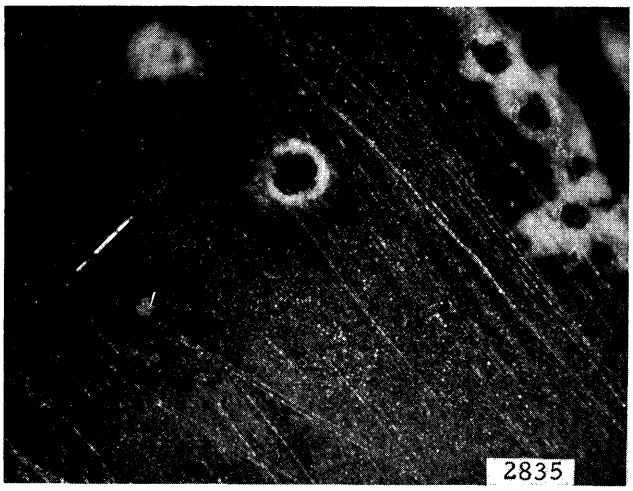

Figure 14. Cavitation Pits in Coated Specimens Showing Material Removal

Figure 15. Cutting Directions on Damaged Specimens

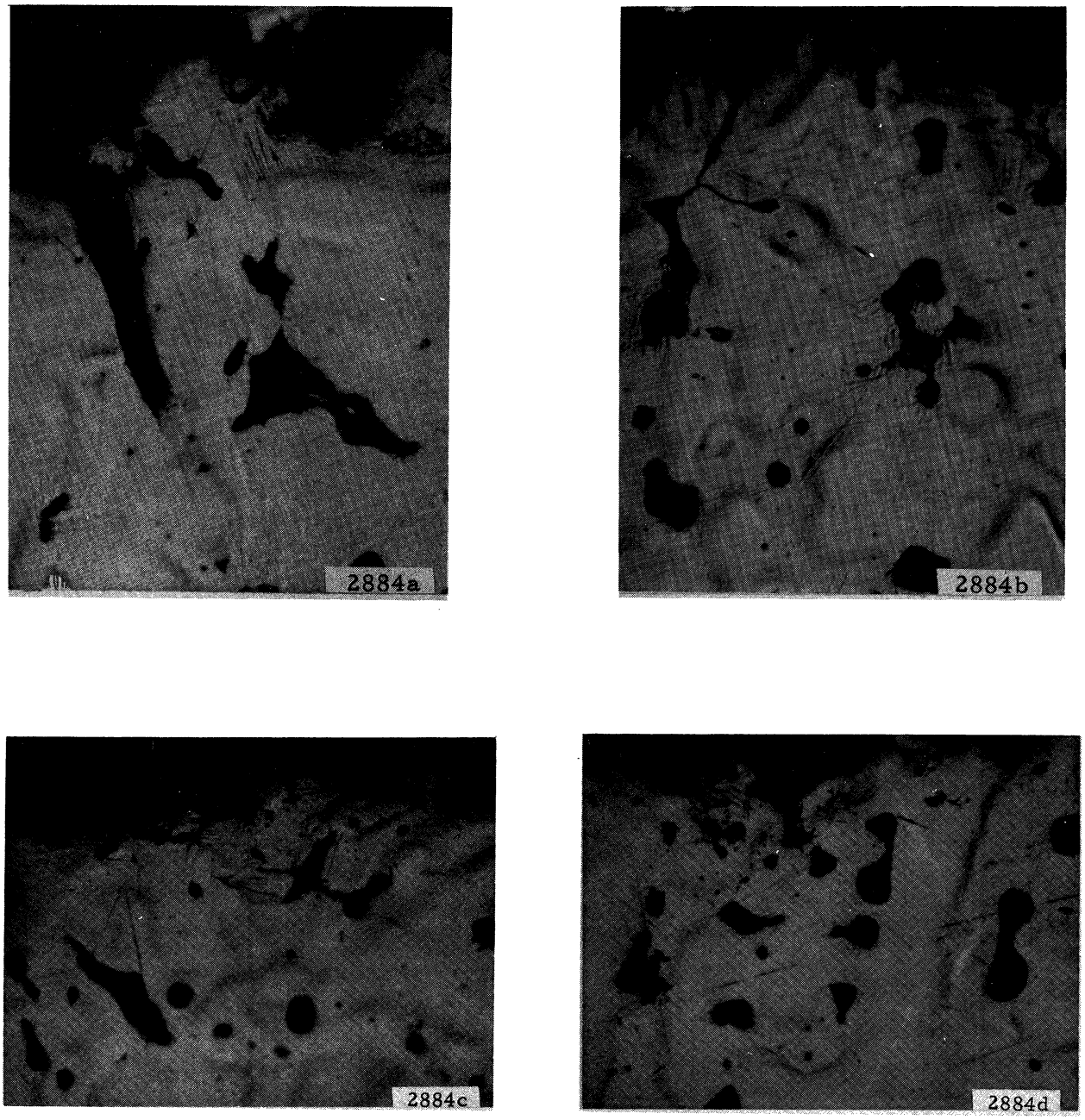

Figure 16. Photomicrographs of Cavitation Damage Area of Zero Load SAE 660 Vibratory Specimens (400x)

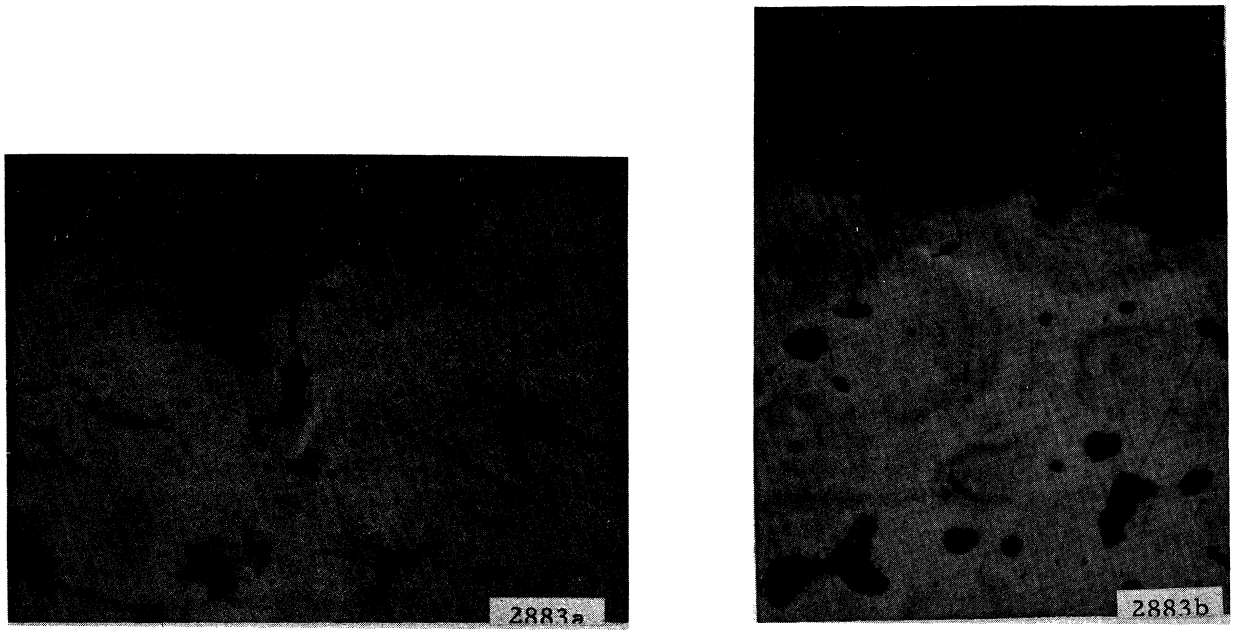

Figure 17. Photomicrographs of Cavitation Damage Area of Tension SAE 660 Vibratory Specimen (400x)

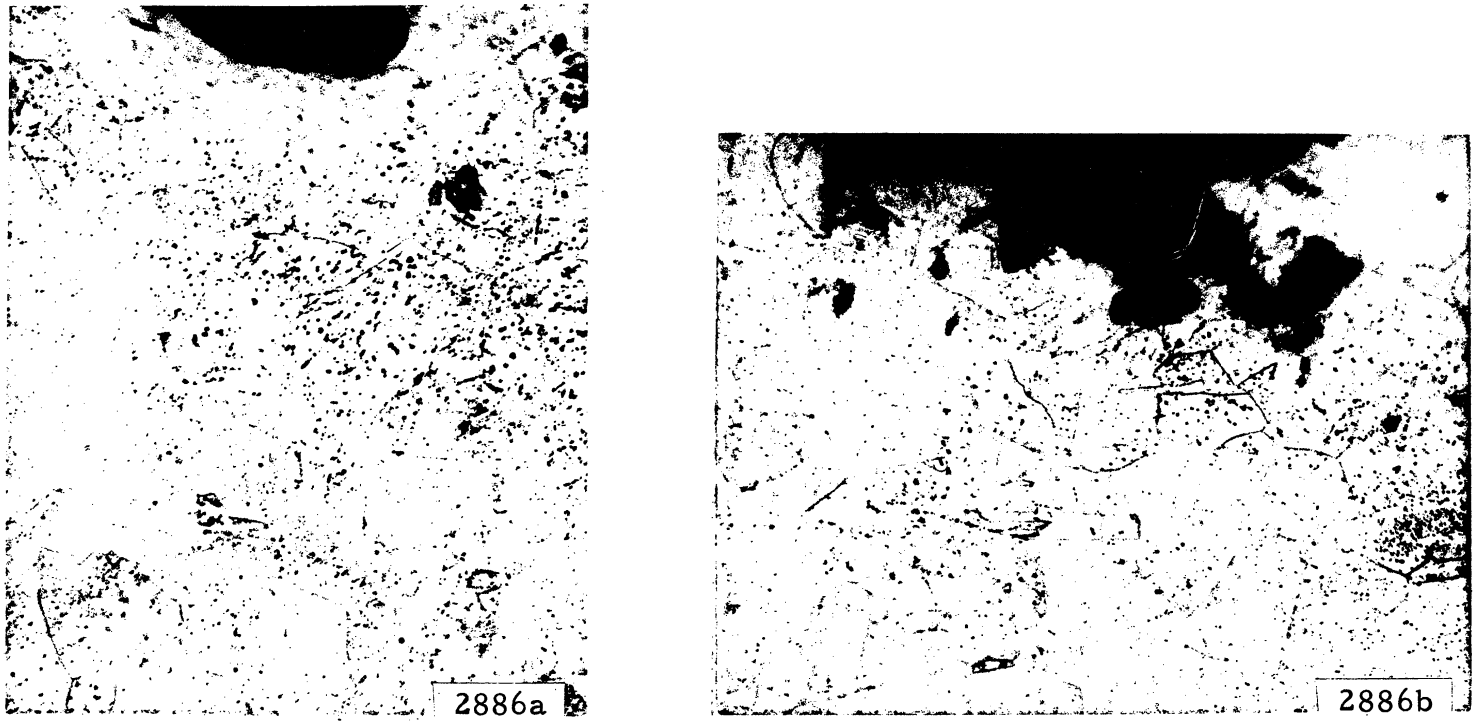

Figure 18. Photomicrographs of Cavitation Damage Area of Tension OFHC Copper Vibratory Specimens (400x)

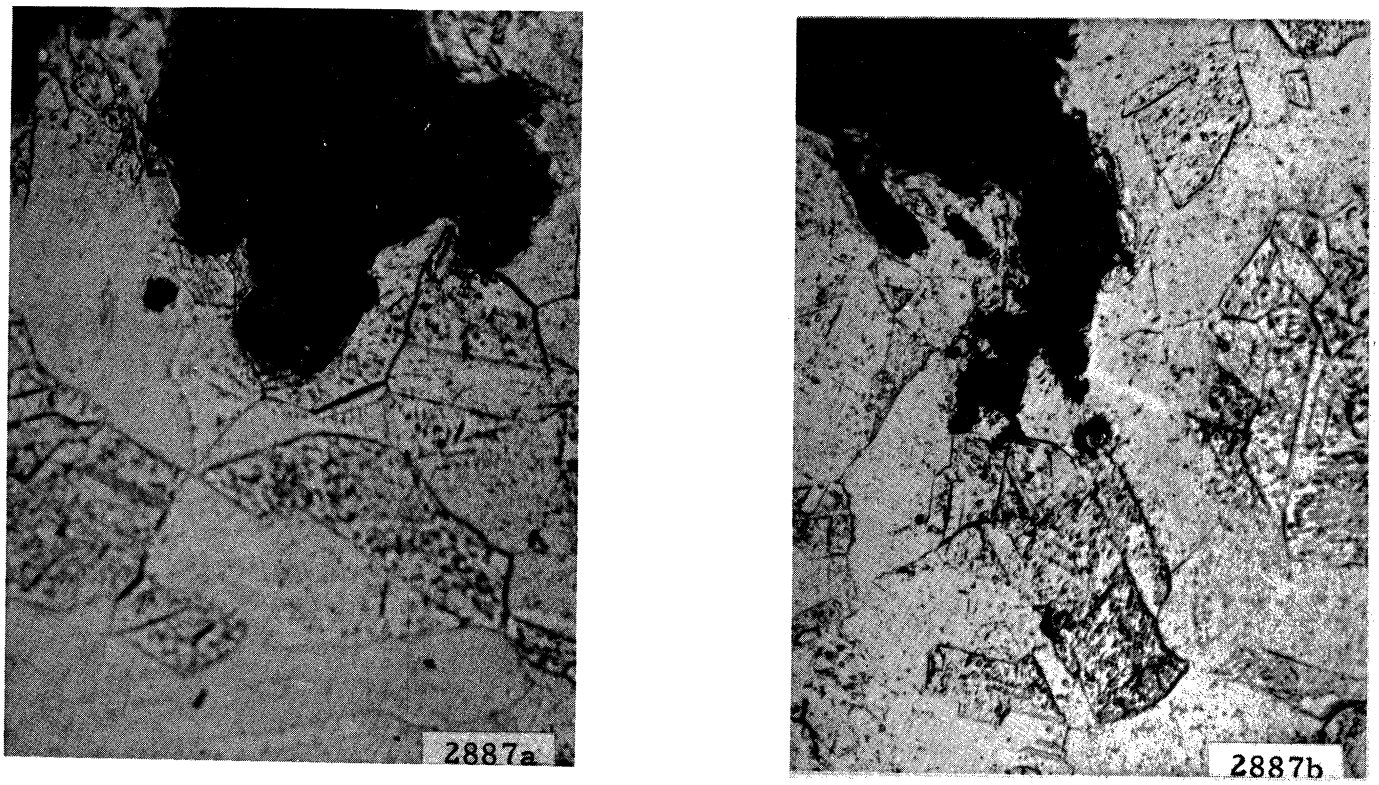

Figure 19. Photomicrographs of Cavitation Damage Area of Compression OFHC Copper Vibratory Specimens (400x)